

Uniform white light distribution with low loss from coloured LEDs using polymer doped polymer mixing rods.

Chris A. Deller, Geoff B. Smith, Jim B. Franklin
Dept. Applied Physics, University of Technology Sydney
P.O Box 123, Broadway 2007 Australia

ABSTRACT

Colour mixing of red, green and blue (RGB) LEDs is demonstrated for a 6 cm long PMMA cylindrical rod with a transparent refractive index matched micro particle (TRIMM) diffuser sheet at the output end. Ray tracing simulations have been performed, and the output light distributions, transmittances and losses modelled and compared with experiment. Photographed and modelled colour mixing results are presented for rods with and without TRIMM sheet mixers. The TRIMM particles homogenize the light output of plain PMMA rods to form white light, with negligible backscattering. A simple method for measuring the concentration of the particles in the diffuser sheet is described, and computer modeling and analysis of TRIMM particle systems is discussed.

1. INTRODUCTION

Mixing rods are used to homogenize light output from multiple sources in devices such as backlit liquid crystal displays and data projectors. Designers want high efficiency and output uniformity in minimum possible size. It has been stated that a length to width ratio of about 10:1 is required to achieve the necessary output light uniformity¹. Shorter lengths are desirable as the size of devices is steadily decreasing.

Mixing rods that rely entirely on total internal reflection (TIR), such as plain PMMA rods, have the disadvantage that undesirable patterns are produced due to caustic effects. It has been reported in a previous study of RGB colour mixing that clear PMMA mixing rods made no significant improvement in illuminance or colour uniformity compared to a bare LED array. A diffuser at the output end significantly improved the output light distribution, but with an additional loss of 6%². Transparent refractive index matched micro (TRIMM) particle mixers homogenize the light output with low loss, because the microsphere particles deviate the light rays by a small amount each interaction, with low backscatter³.

The diffuser sheet used in this experiment consists of cross-linked PMMA spheres (TRIMM particles) embedded in a PMMA matrix. The mean particle size is ~ 35 μm in diameter. A study of the optical properties of similar sheets has been published³. Light transport in polymer optical fibre doped with TRIMM spheres has been reported⁴ and a paper showing uniform colour mixing of RGB light sources using PMMA extruded rods containing TRIMM particles will appear soon⁵. In this study, we incorporated TRIMM particles into the light mixer system in a diffuser sheet at the output end of a clear PMMA rod. There were several reasons for this approach. Firstly, the extruded rods studied previously were not of sufficient optical quality to experimentally ascertain any losses due to the TRIMM particles alone. In addition, the diameter of the rods was too small to use 5mm LED triads as light sources. (Extruded larger diameter rods were not available.) It is also of interest to see how these particles perform as end diffusers, instead of having TRIMM dispersed evenly throughout the rods.

2. EXPERIMENT

Two transparent PMMA rods 25.55 mm in diameter were used in this experiment. A 2.94 mm thick TRIMM diffuser sheet was glued to an end of a 58.95 mm long rod using Loctite IMPRUV[®] 34931 glue. No air bubbles or defects were visible at the interface, which is indicative of a good optical joint. Thus the total length of the rod with TRIMM sheet diffuser is 59.8 mm. The plain PMMA rod (referred to as 'clear') is 61.9 mm long.

The sources that are mixed are two sets of 5 mm RGB LEDs, denoted as Alpha group and Beta group. Each group consists of a triad of 3 LEDs. It is desirable for the individual angular source distributions within a set to be as similar as possible. The LEDs were selected from a larger pool of 5 mm LEDs, all of which had been measured using a photogoniometer described elsewhere³. A cross-section of the angular intensity distribution of the Alpha and Beta group LEDs, as measured by the photogoniometer, is shown in Figure 1. Spectra of the LEDs were obtained via an Ocean Optics SD2000 fiber optic spectrometer coupled to an Oriel 70491 integrating sphere, and associated software. 1931 CIE coordinates for the LEDs were derived from the respective spectral power distributions. These source CIE coordinates and the LED peak spectral wavelengths are given in Table 1.

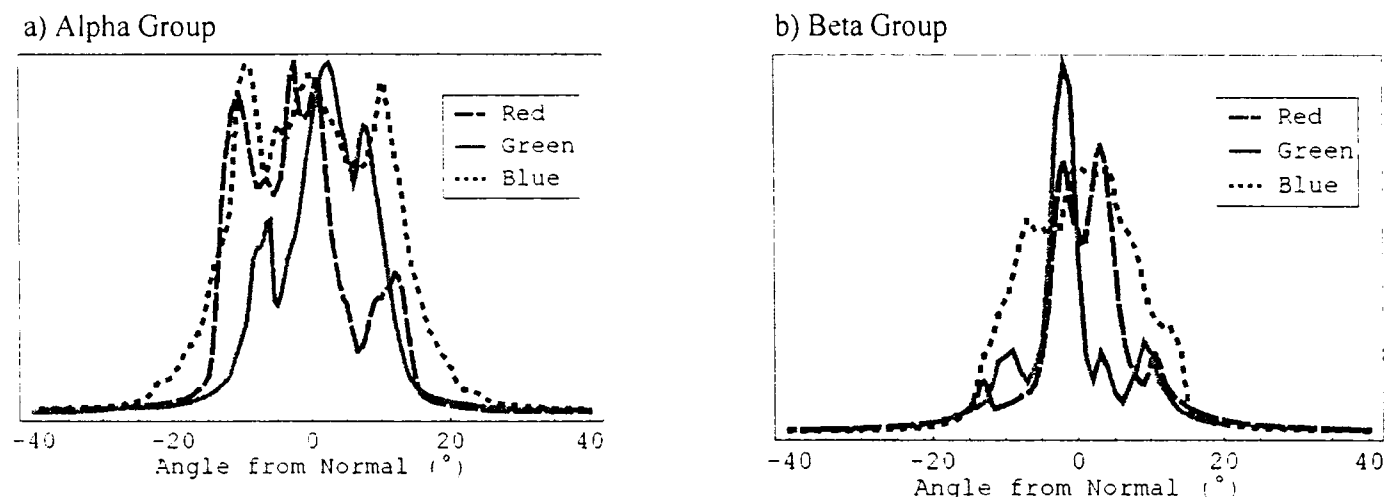


Figure 1. Measured angular distribution of the source LEDs. a) Alpha group b) Beta group

<i>Alpha Group</i>	CIE x	CIE y	<i>Beta Group</i>	CIE x	CIE y
Alpha Red (642nm)	0.701	0.294	Beta Red (632nm)	0.691	0.301
Alpha Green (509nm)	0.114	0.681	Beta Green (513nm)	0.162	0.674
Alpha Blue (462nm)	0.135	0.058	Beta Blue (460nm)	0.138	0.062

Table 1. 1931 CIE coordinates and peak wavelength of the source LEDs, as measured using a spectrometer.

The Alpha group LEDs are better matched in angle than the Beta group, but the Beta group is superior in terms of colour for RGB mixing, as the spectra of the Beta peaks are more widely spread. (The spectral peaks of Alpha green and blue are closer together (Table 1).) For the computer modeling, a separate source model was generated for each LED based on these measured profiles.

The experimental setup for measurements is shown in Figure 2a. The Alpha or Beta RGB LED triad was mounted as close as possible to the end of the mixing rod. The centre point of the LED array was aligned with the rod's axis. A frosted glass screen (dimensions 120 mm x 95.5 mm) was positioned 4 cm or 15 cm from the exit end of the rod. Photographs of the transmitted output distributions were taken with an Olympus C-4000 ZOOM digital camera. Transmittance measurements were performed using the Alpha LED source array and the 'clear' and 'clear + TRIMM diffuser' rods with the output end coupled to the entrance port of an Oriel 70491 integrating sphere. A BPW21 photodiode was attached to the detector port of the integrating sphere, and readings taken with a Data Precision DP 100 Multimeter. The ratio of the transmitted to incident readings were taken using measurements of the bare LED array as the total incident light.

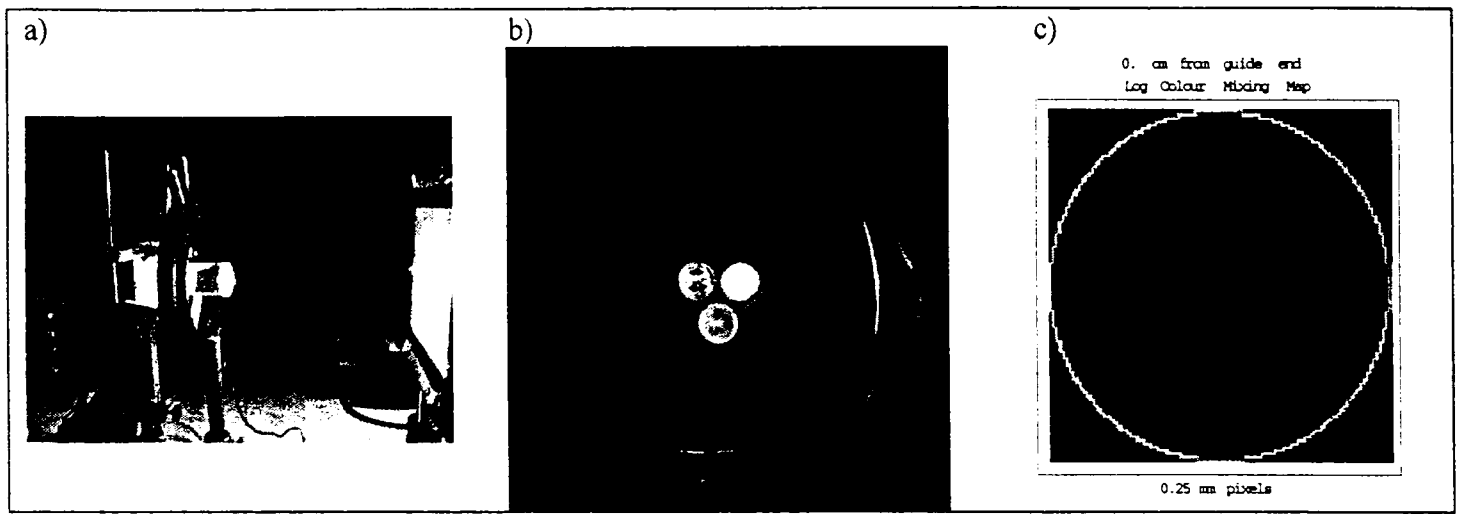


Figure 2. a) experimental setup: LED array, mixing rod, frosted glass screen. b) photograph of Beta LEDs and clear PMMA rod, ~ 20 cm from the rod exit surface, at an off-axis angle to avoid excessive over-exposure. TIR from the rod surfaces is visible. c) modelled clear rod exit end surface illumination of modelled Beta LEDs

3. TRIMM PARTICLES AND MODELING

Ray tracing simulations using 1 million initial rays for each source LED were carried out to model the experimental conditions. The rays were emitted uniformly over a 4 mm diameter area, and measurement-based algorithms were used to realistically simulate the LED light output. Output rays from the end of a rod are traced to modelled 'screens' at predefined distances from the rod exit end. The number of rays that hit each pixel in each modelled screen is recorded. A separate simulation was carried out for each LED, and the RGB results combined for the simulated output intensity and colour distribution. Details and relevant colour calculations have been reported recently⁵. Transmittance and loss data is modelled by counting the number of rays exiting or reflecting from the relevant rod surfaces.

The Monte Carlo ray tracing modeling within a light guide has previously been described elsewhere⁴. The basic concepts are reviewed in Figure 3

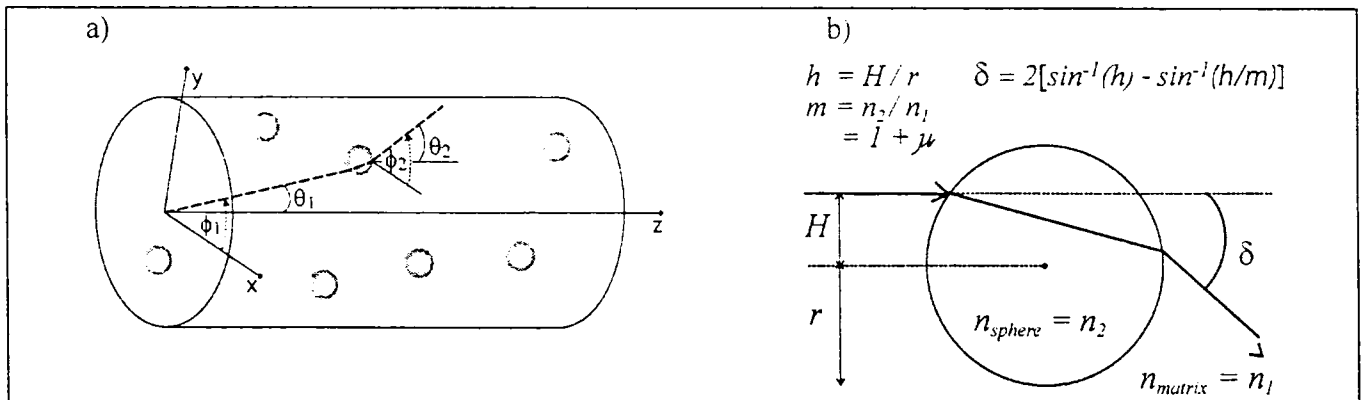


Figure 3. a) Defining ray direction as it propagates along a TRIMM mixing rod. b) Angular deviation of a ray when it strikes a TRIMM sphere. Note that δ is in 3 dimensions, involving a change in both θ and ϕ

The direction of propagation of a ray along a mixing rod is described by the angle, θ , with the light guide axis, z , and the azimuth angle, ϕ as shown in Fig. 1a. Every time a ray strikes a TRIMM particle, there is an angular deviation, δ , shown in Fig. 1b. The ratio h used in the calculation of deviation angle is chosen randomly for each interaction of a ray with a TRIMM sphere, to give uniform probability of impact point. The deviation can be described in terms of geometric optics because the size of the particle is large compared to the wavelength^{3,4}. New θ and ϕ directions for the deviated ray are calculated using 3D spherical geometry after each particle interaction⁴.

The relative refractive index, $m = n_{\text{sphere}}/n_{\text{matrix}}$ can be usefully described by its difference from one; $m = 1 + \mu$. In TRIMM systems $\mu \ll 0.1$, so the deviation angle is small, and back reflectance is $\approx \mu^2/4$, which is negligible. In addition, small changes in n_{matrix} or n_{sphere} can cause large changes in μ and thus the scattering properties of the system². The deviation of a light ray after encountering a TRIMM sphere has been given by

$$\delta = 2 \left[\sin^{-1}(h) - \sin^{-1}\left(\frac{h}{1+\mu}\right) \right] \approx \frac{2\mu h}{\sqrt{1-h^2}} \quad (1)$$

The simplified approximation $2\mu h / \sqrt{1-h^2}$ is derived using a Taylor expansion of $(1+\mu)$, and neglecting higher order terms. The median value of h , the radial fraction of contact of a ray with a sphere, is $1/\sqrt{2}$. Substituting this into Equation (1) the median deviation angle, δ_m , is thus

$$\delta_m = 2\mu \quad (2)$$

For $\mu = 0.011$, $\delta_m = 1.3^\circ$, and for $\mu = 0.018$, $\delta_m = 2.1^\circ$.

The effect of changing m (and therefore μ) has on the distribution of deviation angles is shown in Figure 4. Figure 4a has μ for TRIMM particles in PMMA ($n_1 = 1.490$, $n_2 = 1.507$, $\mu = 0.011$ at 590 nm). It can be seen that most deviations are ~ 1 or 2 degrees. Figure 4b shows the distribution for TRIMM particles in POF matrix, as previously described⁴ ($n_1 = 1.480$, $\mu = 0.018$ at 590 nm).

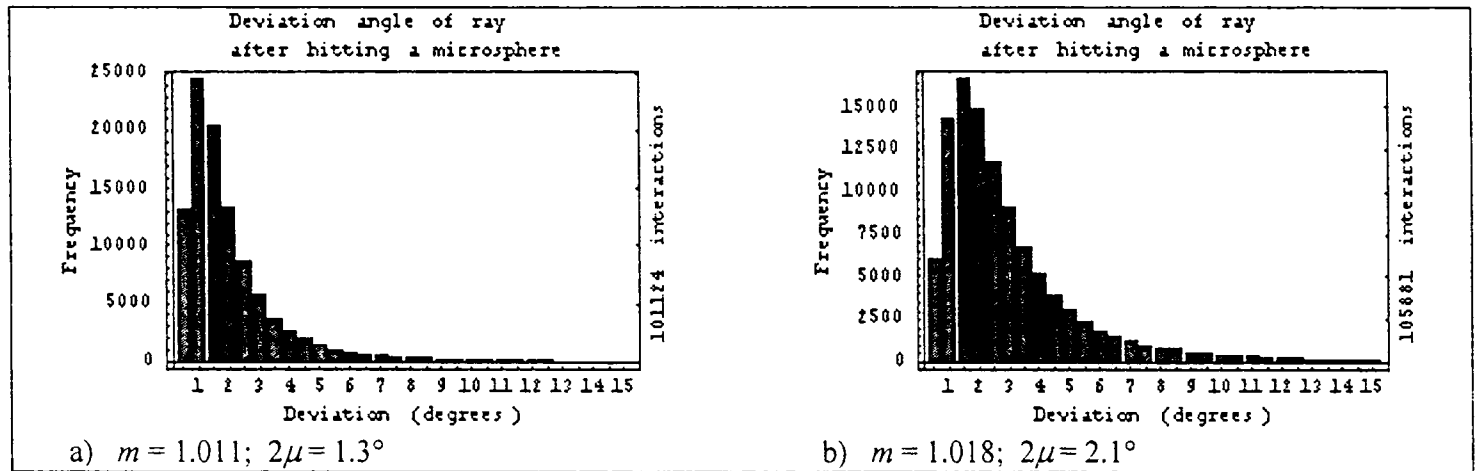


Figure 4. Frequency of deviation angles upon encountering a TRIMM particle for $m = 1.011$, $m = 1.018$

3.1 Determination of TRIMM particle concentration in sheet

The number of particles encountered by a light ray along its path through a TRIMM mixer is related to the volume concentration of the particles in the matrix. For purposes of Monte Carlo computer ray tracing, we need to know the mean distance between particles, l . This was not known for the diffuser sheets used, and had to be measured. We define the axial particle number, a , of a diffuser sheet as the average number of particles that an undeviated ray would encounter when passing through the sample. For a sample of thickness, t , $l = t/a$. So by measuring a , l can be determined.

The probability of an undeviated ray striking a particle as it passes through a sample can be described by a Poisson distribution

$$P(x) = \frac{e^{-\sigma} \sigma^x}{x!} \quad \text{for } x = 0, 1, 2, \dots \quad (3)$$

where σ is the average number of events⁶. The probability of a ray striking zero number of particles when traveling through a sample with axial particle number a is

$$P(0) = e^{-a} = T_{spec} \quad (4)$$

where T_{spec} is the specular transmittance.

3.2 Measurement of axial particle number

Measurement of the true specular transmittance of a particular sample can be used to estimate a . In order to do this, the axial particle number of a particular sample must be small enough to ensure a visible specular component. For $a = 6$, T_{spec} is 0.0025. The concentration of TRIMM particles in the diffuser sheet used is sufficiently high to necessitate measuring thin slices (< 1 mm), so slices were cut from the main sheet using a diamond saw. To ensure optically smooth surfaces for measurement, these slices were mounted between sheets of 2 mm thick PMMA, using glycerol between each of the surfaces as a refractive index matching agent.

A helium neon laser (wavelength 633 nm) was used for the transmittance measurements that were used to calculate a . An advantage of using a laser is the relative ease of being able to see an transmitted undeviated, specular 'spot', indicating that the samples are sufficiently thin for axial particle measurements, as well as making alignment easier. An Oriel 70491 integrating sphere was positioned 3.8 m from the sample, and readings taken using a BPW21 photodiode at the detector port and a multimeter with a resolution of 1 μ W. To estimate a , it is necessary to separate the specular component of transmission from the diffuse. The port size of the integrating sphere was reduced to 1 cm diameter with a cover, making the acceptance criterion for specular transmission within a cone semi-angle of 0.075 degrees. The laser beam was directed through the sample towards the integrating sphere. The component of measured transmittance in the incident beam direction, I_{max} , was measured with the port of the integrating sphere in line with the undeviated beam. This is mainly the specular part of the transmitted beam, but also contains a small scattered component, I_{scatt} . This was subtracted from I_{max} to obtain the specular component of measured intensity. The scattering baseline, I_{scatt} , was estimated by moving the integrating sphere 1, 2, and 3 cm to either side of the central axis, corresponding to median angular deviations of ~ 0.15 , 0.30 and 0.45 degrees, and taking intensity readings. The initial intensity I_0 was measured by directing the laser beam into the integrating sphere through the PMMA and glycerol only. The specular transmittance of the beam through the sample was then calculated by

$$T_{spec} \approx \frac{(I_{max} - I_{scatt})}{I_0} \quad (5)$$

Three sets of measurements were made, using slices of sheet 0.25, 0.27 and 0.33 mm thick, to derive the linear particle concentration of TRIMM in the diffuser sheet. A was calculated for each sample using equation (4), and from this the distance between particles l was calculated to be 0.075 ± 0.005 mm. The TRIMM diffuser sheet thickness is 2.94 mm, giving an axial particle number of 39 ± 3 for this experiment.

3.3 Ray diffusion and angular spread with TRIMM

A ray's path along a TRIMM mixer, as it deviates with every sphere interaction, can be described as a random walk. The half cone angular spread, (Σ) , of the light in the cross-sectional (x-y) plane as it proceeds internally through a TRIMM doped material is dependent on the average deviation and axial particle number

$$\Sigma \approx \delta_m \sqrt{a} \quad (6)$$

For the TRIMM diffuser sheet used here, $\Sigma \approx 1.3^\circ (\sqrt{39}) = 8.1^\circ$. This corresponds to an external half cone spread of $\approx 12.1^\circ$ after refraction upon exiting the guide end. It should be remembered that this spread is in addition to the existing spread inherent in the distribution of the source LEDs, and that the clear rod partially mixes before the sheet.

Sometimes the value of μ cannot be altered because it is set by the materials used. In such cases, axial particle number and rod aspect ratio can be tailored so that total deviation, Σ , will cause the resulting cone of light to spread across the entire end of the mixing rod before exit. This ensures completely homogeneous mixing with no caustics formed.

3.4 Rotational symmetry and statistical analysis

Caustics are often formed when light mixing is performed relying on TIR only, using clear undoped PMMA rods. These can be removed by adding a TRIMM diffuser to the end of a clear rod, or having TRIMM dispersed within the mixing rod. There may be cases where it is desirable to keep the TRIMM concentration low to avoid side loss³, say if μ is large, meaning δ_m will be larger (equation (2) and Figure 4). High angular spread of the source distribution can be another reason for keeping the TRIMM particle concentration as low as possible. The chief geometrical factors affecting the degree of caustics formation in a clear rod, apart from the source distribution, are: 1) rod length to diameter aspect ratio (AR), and 2) the relative radial source distance of the LEDs from the rod axis (source radial fraction, see Figure 5a). Computer modeling is useful for optimizing these factors to minimize caustics formed purely due to system geometry, and for determining the optimal TRIMM concentration needed to homogenize the light output.

For the computer modeling of colour mixing, at least 3 sets of data, one for each LED, is generated for a particular simulated screen to rod distance. The 3 data sets are added together to form a complete colour map⁵. If the modelled mixing rod output intensity from a single LED projected onto a simulated screen is not rotationally symmetric, then the final colour mixing will be uneven. Statistical analysis of modelled data can show how rotationally symmetric the projected output intensity will be. This gives an indication of whether bright caustics will be formed in an undoped rod, and if TRIMM concentration is sufficient to cause complete and uniform colour mixing in a TRIMM mixing rod. This type of analysis also aids in system design, as AR and source radial fraction can be optimized to give uniform light distribution for a given μ and TRIMM concentration.

Modelled rays exiting a mixing rod for a single LED are projected onto a pixellated screen. The value of each pixel contains a number, corresponding to the number of times it has been struck by an output ray. This data is used to perform rotational symmetry statistical analysis. Figure 5 shows the concept of arranging the pixels into 'bins' of equal radial intervals from the centre of the simulated screen. The average number of rays per pixel, and the standard deviation, is calculated for each 'radial bin'. This data, plotted against the radial distance from the centre of the 'screen', is a good measure of the rotational symmetry of the light output.

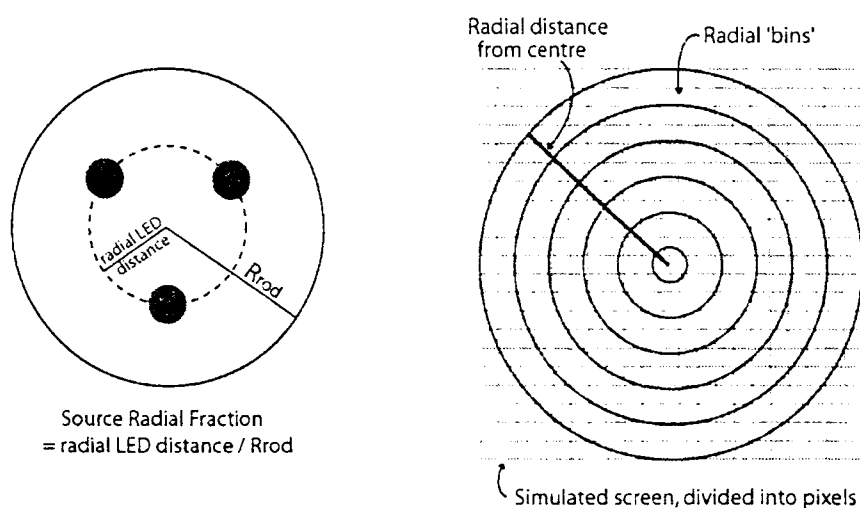


Figure 5. a) Schematic showing entrance end of mixing rod, with relative positions of the LEDs to the rod axis (centre) and rod radius. b) Pixels in a simulated 'screen' are sorted into radial 'bins' for analysis of rotational symmetry of output light distribution.

4. RESULTS

4.1. Colour Mixing Results

Modelled and photographed results of the output light from the Alpha group LED triad, projected onto a screen 15 cm from the end of the mixing rods, are shown in Figure 6 and 7. Figure 6 shows the colour distribution when using the clear PMMA rod only as the mixer. Figure 7 shows the distribution from the rod with TRIMM diffuser sheet.

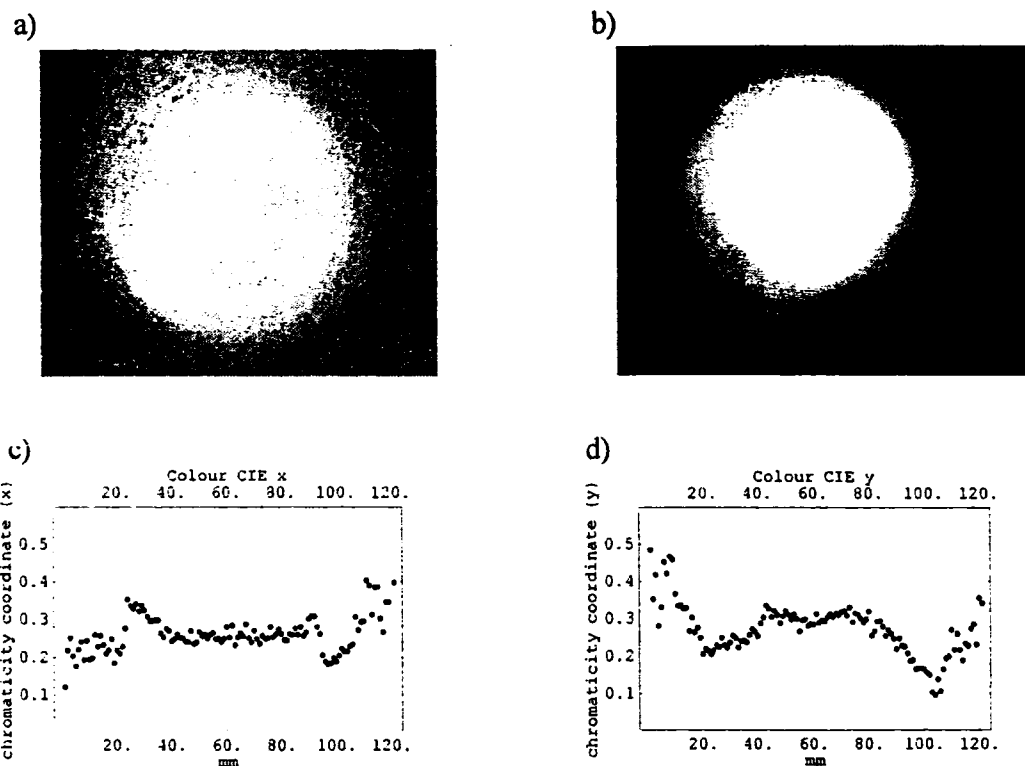


Figure 6. a,b) Output colour distribution transmitted through the frosted glass screen 15cm from the end of the clear PMMA rod. a) modelled. b) photographed. c,d) Modelled CIE coordinates of a horizontal strip through the centre of the screen. c) CIE x d) CIE y

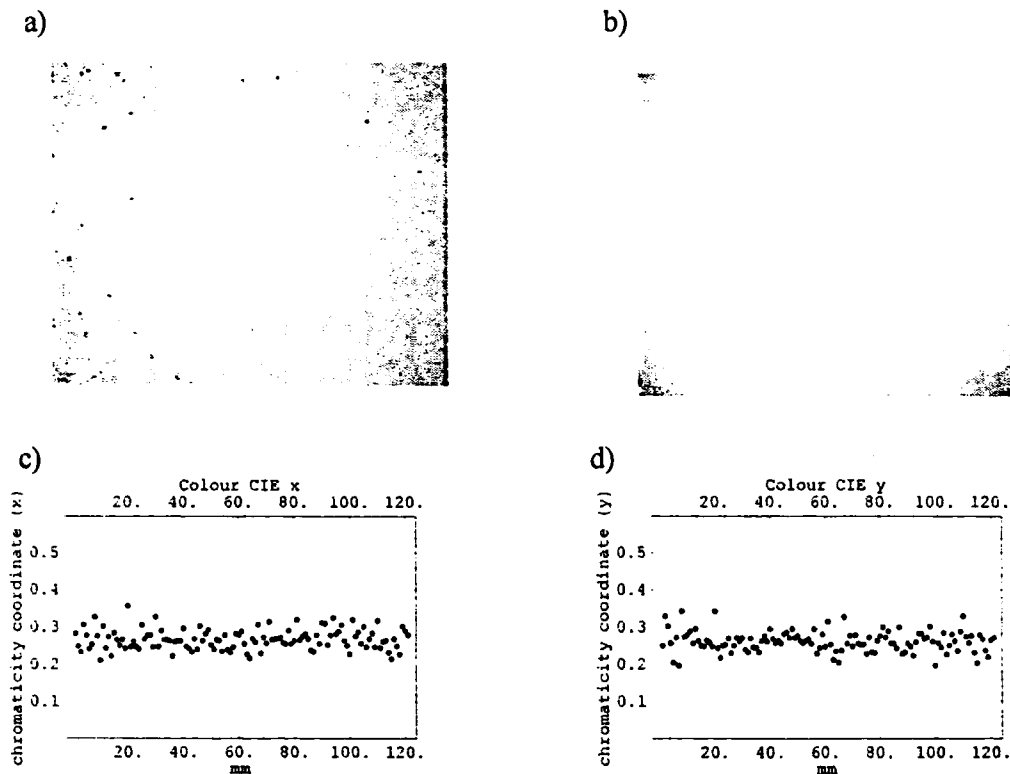


Figure 7. a,b) Output colour distribution transmitted through the frosted glass screen 15cm from the end of the clear PMMA rod. a) modelled. b) photographed. c,d) Modelled CIE coordinates of a horizontal strip through the centre of the screen. c) CIE x d) CIE y

The photographed and modelled images are both 120 mm x 95.5 mm. Each pixel in the modelled screens represents 1 mm². Excellent quantitative agreement between the measured and modelled CIE x and y coordinates derived from colour output from mixing rods, and from corresponding modelled colour output, has been demonstrated in a recent study⁵. CIE coordinates from modelled results only are shown here.

An artefact of the photographs is the inability to display colour over a large brightness range. The colours on the outer periphery of Figure 6b actually appear brighter when viewed with the eye. Similarly, the blue halo in Figure 7b, although slightly visible in the experimental system, appears much lighter to the eye. In addition, it was difficult to generate a sufficiently high intensity from the green LED to achieve a desirable colour balance, as is evident in both the modelled and photographed results. It can be seen, however, that a uniform colour is obtained across the screen, because, as Figures 7 c and d indicate, the CIE plots of the rod + diffuser sheet results are constant.

4.2. Transmittance & Losses

The fate of rays can be categorized as detailed in Figure 8 in terms of key surfaces and ray directions at the surface. Results are given for measured and modelled mixing of the Alpha LED array with clear 6 cm rod, and for PMMA rod with TRIMM mixer. **A⁻** refers to the fraction of rays incident on the entrance end of the rod that are Fresnel reflected. **B⁻** is the fraction of incident light (**I₀**) reflected from the end surface which is ‘lost’, most of which is transmitted out through the source end of the mixer. **C⁺** is the percentage of **I₀** transmitted out of the end surface. Light transmitted out of the side edges of the diffuser TRIMM sheet, in any direction, is given by **D**. (For a clear rod, **D** is negligible.)

Transmittance measurements made for the individual red, green and blue LEDs were averaged, and compared with similarly averaged transmittances obtained from simulation data. The results are shown in Table 2. The measured output from the TRIMM sides (**D**) was obtained by difference, by taking readings with the diffuser in and out of the integrating

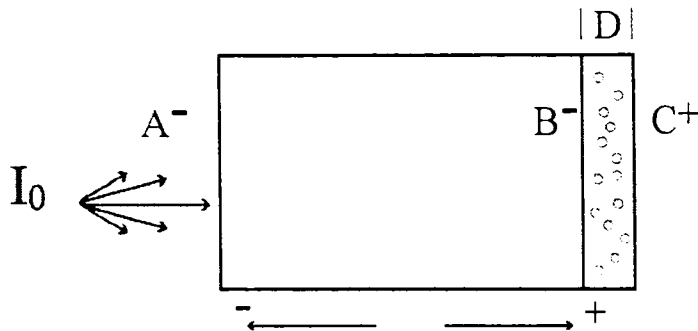


Figure 8. Schematic of mixer rod, showing surfaces for which a transmittance or reflected loss is shown in Table 2.

		<i>Clear PMMA rod</i>		<i>Clear rod + TRIMM diffuser</i>	
		Simulated	Measured	Simulated	Measured
Input Fresnel reflection losses	A⁻	5.7	-	5.7	-
Output end Fresnel losses	B⁻	4.7	-	6.0	-
Forward useful output	C⁺	89.6	87	83.9	83*
Lateral useful output	D	N/A	N/A	4.4	6.0

Table 2. Simulated and measured Transmittance and loss results, as a percentage of the incident light, for Alpha group LEDs, for 6cm PMMA mixing rod with and without TRIMM diffuser. *measurement has higher uncertainty (see text)

sphere. The measured transmitted end light for the rod + TRIMM mixer has a higher uncertainty than the other measurements. This is because measurements using integrating spheres can only be accurately compared when the angular spread of the light is comparable. The TRIMM diffusers used here produce an additional half-cone angular spread of about 12° compared to the clear rods (equation (6)), so a correction factor was estimated to account for the effect that this difference has on readings obtained using the integrating sphere. This correction factor was obtained by making measurements of the transmitted light from the LED array through a diffuser sheet alone, compared with estimates based on previous measurements with two spectrophometers using a narrow collimated beam³.

4.3. Rotational symmetry

The average number of rays per pixel for each radial 'bin' is plotted against the radial distance from the centre of a modelled screen in Figure 9a. The screen was modelled at 15 cm away from the end of the clear rod for the Alpha red LED. If 3 matrices of different colour are to be 'mixed', there must be no sudden 'spikes' or variations in the intensity of the individual LED outputs with screen radius, for uniform colour mixing to be obtained. Figure 9b shows the standard deviation divided by the average rays per pixel for the same data as Figure 9a. The 'expected' values are those expected purely due to statistical fluctuations within the data due to the finite number of rays traced. It is evident that the light distribution is not uniform across the screen, and that if colour mixing were attempted with distributions such as these, caustics would be formed. Figure 9c & d, show the analysis of the same system modelled through the rod with TRIMM diffuser sheet. It can be seen that the light distribution has been smoothed, and caustics will not result in this case.

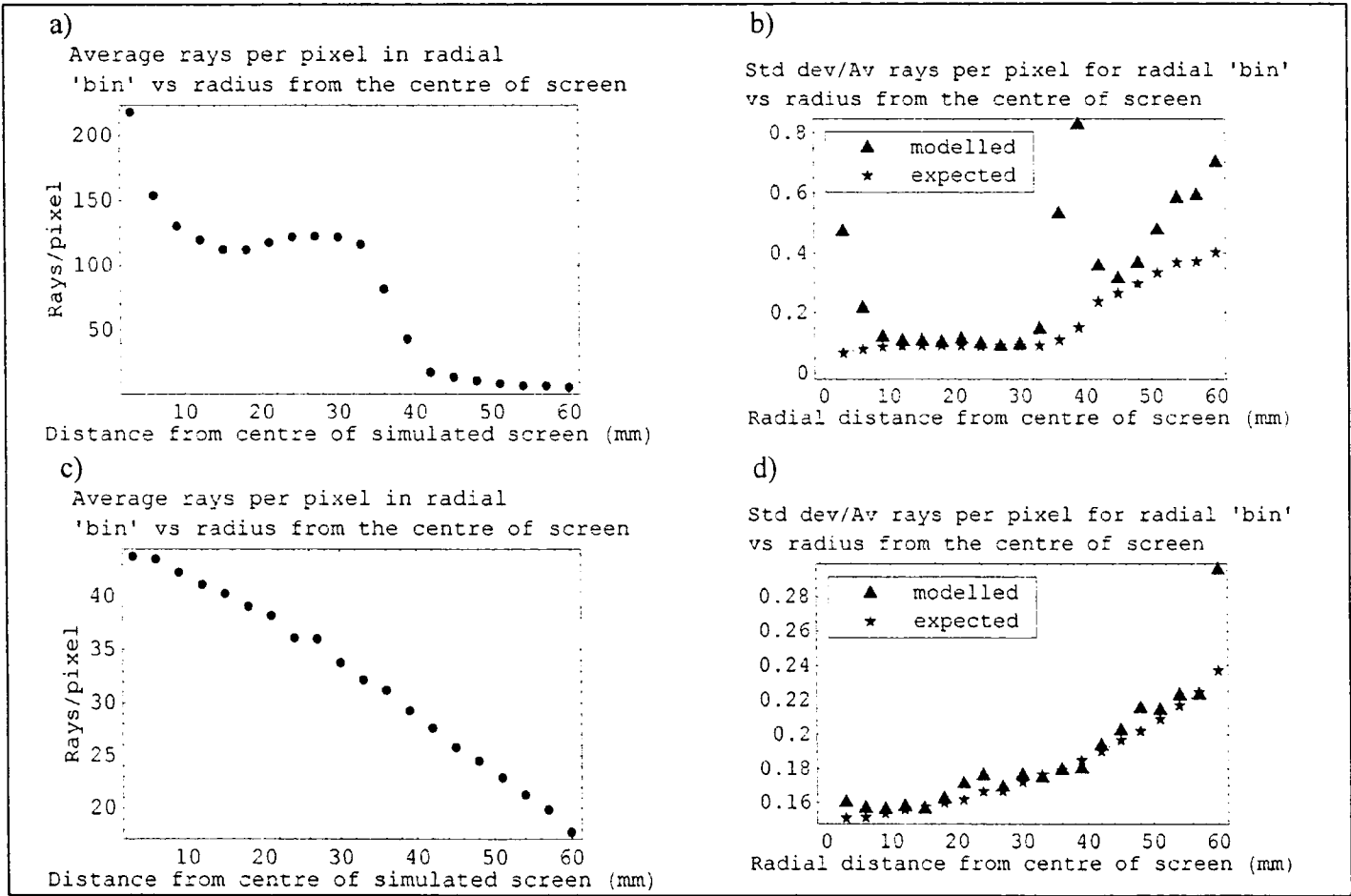


Figure 9 a,b) analysis of simulated ray tracing data projected onto a screen 15cm from the end of the 6cm clear PMMA rod, with Alpha Red LED as the source. a) Average rays per pixel in a 'radial bin' vs radial distance from the centre of the screen (see Figure 5b) b) std deviation/average rays per pixel in a 'radial bin' vs radial distance from screen centre. c,d) similar analysis for PMMA rod with TRIMM diffuser. Outlying point in modelled data due to very small number of rays hitting screen edge.

Proceedings of SPIE on CD-ROM

SPIE Annual Meeting 2004: Optical Systems Engineering

*2–6 August 2004
Denver, Colorado USA*

Proceedings of SPIE
Volumes 5523–5532

Single-User Edition

Proceedings of SPIE on CD-ROM

SPIE Annual Meeting 2004: Optical Systems Engineering

*2–6 August 2004, Denver, Colorado USA
Proceedings of SPIE Volumes 5523–5532*

- 5523: **Current Developments in Lens Design and Optical Engineering V**
- 5524: **Novel Optical Systems Design and Optimization VII**
- 5525: **Laser Beam Shaping V**
- 5526: **Optical Systems Degradation, Contamination, and Stray Light: Effects, Measurements, and Control**
- 5527: **Advances in Thin Film Coatings for Optical Applications**
- 5528: **Space Systems Engineering and Optical Alignment Mechanisms**
- 5529: **Nonimaging Optics and Efficient Illumination Systems**
- 5530: **Fourth International Conference on Solid State Lighting**
- 5531: **Interferometry XII: Techniques and Analysis**
- 5532: **Interferometry XII: Applications**



The International Society
for Optical Engineering

© Society of Photo-Optical Instrumentation Engineers, SPIE
SPIE, P.O. Box 10, 1000 20th Street, Bellingham, Washington, 98227-0010
Tel: +1 360 676 3290 • Fax: +1 360 647 1445 • E-mail: spie@spie.org • Web: spie.org



The papers included in this volume were part of the technical conference cited on the cover and title page. Papers were selected and subject to review by the editors and conference program committee. Some conference presentations may not be available for publication. The papers published in these proceedings reflect the work and thoughts of the authors and are published herein as submitted. The publisher is not responsible for the validity of the information or for any outcomes resulting from reliance thereon.

Please use the following format to cite material from this book:

Author(s), "Title of Paper," in *Complex Mediums V: Light and Complexity*, edited by Martin W. McCall, Graeme Dewar, Proceedings of SPIE Vol. 5508 (SPIE, Bellingham, WA, 2004) page numbers.

ISSN 0277-786X
ISBN 0-8194-5446-X

Published by
SPIE—The International Society for Optical Engineering
P.O. Box 10, Bellingham, Washington 98227-0010 USA
Telephone 1 360/676-3290 (Pacific Time) • Fax 1 360/647-1445
<http://www.spie.org>

Copyright © 2004, The Society of Photo-Optical Instrumentation Engineers

The papers published in these proceedings reflect the work and thoughts of the authors and are published herein as submitted. The publisher is not responsible for the validity of the information or for any outcomes resulting from reliance thereon.

Copying of material in this book for internal or personal use, or for the internal or personal use of specific clients, beyond the fair use provisions granted by the U.S. Copyright Law is authorized by SPIE subject to payment of copying fees. The Transactional Reporting Service base fee for this volume is \$15.00 per article (or portion thereof), which should be paid directly to the Copyright Clearance Center (CCC), 222 Rosewood Drive, Danvers, MA 01923. Payment may also be made electronically through CCC Online at <http://www.copyright.com>. Other copying for republication, resale, advertising or promotion, or any form of systematic or multiple reproduction of any material in this book is prohibited except with permission in writing from the publisher. The CCC fee code is 0277-786X/04/\$15.00.

Printed in the United States of America.

Volume 5530 Fourth International Conference on Solid State Lighting

Chairs/Editors: Ian T. Ferguson, Nadarajah Narendran, Steven P. DenBaars, John C.

Carrano

Conference Committee

Introduction

OVERVIEW

Accelerating the development of next-generation solid-state lighting sources [5530-1]

J. Brodrick, C. Christy

Overview: present status and future prospect of system and design in white LED lighting technologies

[5530-3]

T. Taguchi

Triple-doped white organic light-emitting devices grown in vacuum [5530-50]

B. D'Andrade, R. Holmes, S. Forrest, J. Li, M. Thompson

LED APPLICATIONS

An examination of a prototype LED fire-alarm signaling appliance [5530-4]

J. Curran, S. Keeney

SOURCES I

Device performance of AlGaIn-based 240–300-nm deep UV LEDs [5530-5]

A. Fischer, A. Allerman, M. Crawford, K. Bogart, S. Lee, R. Kaplar, W. Chow

Growth and characterization of blue and near-ultraviolet light-emitting diodes on bulk GaN [5530-6]

X. Cao, S. LeBoeuf, S. Arthur, D. Merfeld, M. D'Evelyn

Mg-doped Al-rich AlGaIn alloys for deep UV emitters [5530-7]

M. Nakarmi, K. Kim, K. Zhu, J. Lin, H. Jiang

Performance and application of high-power ultraviolet AlGaInN light-emitting diodes [5530-8]

J. Han, S. Jeon, M. Gherasimova, J. Su, G. Cui, H. Peng, E. Makarona, Y. He, Y. Song,

A. Nurmikko, L. Zhou,

W. Goetz, M. Krames

CHARACTERIZATION

LED photometric calibrations at the National Institute of Standards and

Technology and future measurement

needs of LEDs [5530-10]

C. Miller, Y. Zong, Y. Ohno

LED white light visual equivalence [5530-11]

C. You

Color rendering and luminous efficacy of white LED spectra [5530-12]

Y. Ohno

Rapid photo-goniometric technique for LED emission characterization [5530-13]

P. Boher, M. Luet, T. Leroux

Position-dependent analysis of light extraction of GaN-based LEDs [5530-14]

C. Sun, T. Lee, C. Lin

White LED performance [5530-15]

Y. Gu, N. Narendran, J. Freyssinier

SYSTEMS I

A massive primary approach to solid state lighting [5530-18]

S. Paolini

LED illumination control and color mixing with Engineered Diffusers [5530-19]

T. Sales, S. Chakmakjian, D. Schertler, G. Morris

Application of high-brightness LEDs in aircraft position lights [5530-20]

N. Machi, S. Mangum, J. Singer

A spectrally tunable solid-state source for radiometric, photometric, and colorimetric applications [5530-21]

I. Fryc, S. Brown, G. Eppeldauer, Y. Ohno

SYSTEMS II

Investigation of the spectral properties of LED-based MR16s for general illumination [5530-53]

D. Brown, D. Nicol, A. Payne, I. Ferguson

High-power LEDs for plant cultivation [5530-24]

G. Tamulaitis, P. Duchovskis, Z. Bliznikas, K. Breive, R. Ulinskaite, A. Brazaityte, A. Novickovas, A. Zukauskas,

M. Shur

Applications of deep UV LEDs to chemical and biological sensing [5530-25]

P. Dasgupta, Q. Li, H. Temkin, M. Crawford, A. Fischer, A. Allerman, K. Bogart, S. Lee

Short-range communication with ultraviolet LEDs [5530-49]

A. Siegel, G. Shaw, J. Model

PROCESSING/PACKAGING

Emerging low-cost LED thermal management materials [5530-27]

C. Zweben

Bevelled-sidewalls formation and its effect on the light output of GaInN MQW LED chips [5530-28]

J. Hsu, C. Huang, W. Yeh, J. Tsay, Y. Guo, C. Chuo, C. Lin, C. Sun, S. Pan

Chip-scale thermal management of high-brightness LED packages [5530-29]

M. Arik, S. Weaver

SOURCES II

Deep-ultraviolet LEDs fabricated in AlInGaN using MEMOCVD [5530-30]

M. Khan

Uniform white light distribution with low loss from colored LEDs using polymer-doped polymer mixing rods [5530-32]

C. Deller, G. Smith, J. Franklin

III-nitride blue and UV photonic-crystal light-emitting diodes [5530-33]

J. Shakya, K. Kim, T. Oder, J. Lin, H. Jiang

Study of short-term instabilities of InGaN/GaN light-emitting diodes by means of capacitance-voltage

measurements and deep-level transient spectroscopy [5530-36]

G. Meneghesso, M. Meneghini, S. Levada, E. Zanoni, A. Cavallini, A. Castaldini, V.

Harle, T. Zahner, U. Zehnder

PHOSPHORS

High CRI phosphor blends for near-UV LED lamps [5530-37]

E. Radkov, A. Setlur, Z. Brown, J. Reginelli

Performance of phosphor-coated LED optics in ray trace simulations [5530-40]

A. Borbely, S. Johnson

Concentration and crystallite size dependence of the photoluminescence in YAG:Ce nanophosphor³⁺
[5530-39]

R. Ovalle, A. Arredondo, L. Diaz-Torres, P. Salas, C. Angeles, R. Rodriguez, M. Meneses, E. De la Rosa

RENEWABLE

Successful design of PV power systems for solid-state lighting applications [5530-41]

J. Thornton, B. Stafford

Performance of PV-powered LED lighting systems for buildings [5530-42]

Y. Zhou, N. Narendran

Group III-nitride alloys as photovoltaic materials [5530-43]

J. Ager III, J. Wu, K. Yu, R. Jones, S. Li, W. Walukiewicz, E. Haller, H. Lu, W. Schaff

Growing pains for new energy-saving technologies [5530-44]

S. Kurtz

Effects of ordering on the optical properties of GaInP [5530-45] ²

D. Levi, J. Geisz, B. Johs

POSTER SESSION

Electrode design for InGaN/sapphire LEDs based on multiple thin ohmic-metal patches [5530-46]

S. Lee

Color perception under illumination by quadrichromatic solid-state lamp [5530-47]

R. Stanikunas, H. Vaitkevicius, A. Svezda, V. Viliunas, Z. Bliznikas, K. Breive, R. Vaicekauskas, A. Novickovas,

G. Kurilcik, A. Zukauskas, R. Gaska, M. Shur

White organic light-emitting diodes with high efficiency and stable color coordinates [5530-48]

C. Lee, N. Lee, J. Song, D. Hwang

Conference Committee

Symposium Chair

David L. Begley, Ball Aerospace & Technologies Corporation (USA)

Program Chair

Ian T. Ferguson, Georgia Institute of Technology (USA)

Conference Chairs

Ian T. Ferguson, Georgia Institute of Technology (USA)

Nadarajah Narendran, Rensselaer Polytechnic Institute (USA)

Steven P. DenBaars, University of California/Santa Barbara (USA)

John C. Carrano, DARPA (USA)

Program Committee

Srinath K. Aanegola, GELcore LLC (USA)

William J. Cassarly, Optical Research Associates (USA)

Lianghui Chen, Institute of Semiconductors (China)

Makarand H. Chipalkatti, OSRAM Opto Semiconductors GmbH (USA)

Kevin J. Dowling, Color Kinetics Inc. (USA)

Ivan Eliashevich, Gelcore LLC (USA)
Volker Härle, OSRAM Opto Semiconductors GmbH (Germany)
Stephen G. Johnson, Lawrence Berkeley National Laboratory (USA)
Bernd Keller, Cree Lighting (USA)
Kevin F. Leadford, Lithonia Lighting (USA)
Yung-Sheng Liu, Industrial Technology Research Institute (Taiwan)
Paul S. Martin, Lumileds Lighting, LLC (USA)
Shuji Nakamura, University of California/Santa Barbara (USA)
Seong-Ju Park, Kwangju Institute of Science and Technology (South Korea)
Yoon-Soo Park, Seoul National University (South Korea)
E. Fred Schubert, Rensselaer Polytechnic Institute (USA)
Jerry A. Simmons, Sandia National Laboratory (USA)
Cheolsoo Sone, Samsung Advanced Institute of Technology (South Korea)
Robert V. Steele, Strategies Unlimited (USA)
Tsunemasa Taguchi, Yamaguchi University (Japan)
Brent K. Wagner, Georgia Institute of Technology (USA)

Session Chairs

1 Overview

Ian T. Ferguson, Georgia Institute of Technology (USA)

vii

2 LED Applications

Juan Carlos Miñano, Universidad Politécnica de Madrid (Spain)

3 Organic Solid State Lighting

Ghassan E. Jabbour, Arizona State University (USA)

4 Sources I

John C. Carrano, DARPA (USA)

5 Characterization

Steven P. DenBaars, University of California/Santa Barbara (USA)

6 Systems I

Kevin F. Leadford, Lithonia Lighting (USA)

7 Systems II

Ian T. Ferguson, Georgia Institute of Technology (USA)

8 Processing/Packaging

Edward D. Petrow, Lincoln Technical Services (USA)

9 Sources II

Chris L. Bohler, GELcore LLC (USA)

10 Phosphors

Christopher J. Summers, Georgia Institute of Technology (USA)

11 Renewable

Christiana Honsberg, Georgia Institute of Technology (USA)

viii

Introduction

This Fourth International Conference on Solid State Lighting took place during the SPIE Annual Meeting in Denver, Colorado on August 3-6, 2004.

Contained in these proceedings are submitted papers of 40 invited and contributing attendees of this meeting. The topics covered by these papers range from light measurement and characterization standards to LED processing techniques to the possible applications of solid state light sources. It is evident from the quantity and quality of these proceedings that solid state lighting, as a technology, and an industry is a rapidly developing area of science and technology.

The conference chairs would like to thank SPIE for hosting this meeting, as well as the program committee members, authors, and session chairs for making this meeting a technical success that provides valued and timely research on Solid State Lighting.

Ian T. Ferguson

Nadarajah Narendran

Steven P. DenBaars

John C. Carrano